

An iterative local-updating ensemble smoother for high-dimensional inverse modeling with multimodal distributions

Jiangjiang Zhang^a, Guang Lin^b, Weixuan Li^c, Lingzao Zeng^a, Laosheng Wu^d

^a College of Environmental and Resource Sciences, Zhejiang University, Hangzhou, 310058, China,

^b Department of Mathematics & School of Mechanical Engineering, Purdue University, West Lafayette, IN 47907, USA,

^c Pacific Northwest National Laboratory, Richland, WA 99352, USA,

^d Department of Environmental Sciences, University of California, Riverside, CA 92521, USA.

Abstract

Ensemble smoother (ES) has been widely used in high-dimensional inverse modeling. However, its applicability is constrained by the requirement of Gaussian distribution of model parameters. For problems with multimodal distributions, using ES directly is problematic. One solution is to adopt clustering analysis to identify each mode, which is not very efficient when the dimension is high or the number of modes is large. In this paper, free from clustering analysis, we propose a very simple while efficient algorithm, which is entitled the iterative local-updating ensemble smoother (ILUES), to efficiently explore multimodal distributions in high-dimensional problems. This algorithm is based on updating local ensembles of each sample in ES to explore possible multimodal distributions. To guarantee the performance in nonlinear problems, we adopt an iterative form of ES to assimilate the measurements multiple times. Four numerical case studies are tested to show the performance of the proposed method. The first example is a simple one that has infinite modes in the posterior distribution, which is used to illustrate the basic ideas of the proposed method. To show its applicability in practical problems, we test the ILUES algorithm with three inverse problems in hydrological modeling with multimodal prior distribution, multimodal posterior distribution and a large number of unknown parameters, respectively.

Keywords

Ensemble smoother; Inverse modeling; Parameter estimation; Multimodal distribution

1. Introduction

Parameter identification is an important aspect in uncertainty quantification of physical systems. However, the direct measurement of model parameters is usually difficult or even impossible in many cases. In this situation, to obtain an estimate of the model parameters, we need to solve an inverse problem with the information provided by some indirect measurements (hereinafter referred to as measurements). The approaches to solving an inverse problem can be grouped into two categories, i.e., the deterministic and stochastic ones. The deterministic approach seeks to find a set of model parameters that best fits the measurements by solving an optimization problem, which can be realized with local (e.g., the Levenberg-Marquardt algorithm [1]) or global (e.g., the genetic algorithm [2]) search algorithms. As there always exist different combinations of parameter values that all can well fit the measurements, i.e., the inverse solution is not unique, obtaining only one most favored solution would ignore the uncertainties of model parameters. To fully consider the parametric uncertainties, we can adopt the stochastic approach and model the parameters as random variables.

In the Bayesian framework, the uncertainties of parameter estimation are represented with the posterior distribution, from which we can obtain any desired statistics [3]. According to Bayes' theorem, the posterior distribution is proportional to the product of the prior distribution and the likelihood. Except for a few simple cases, the analytical form of the posterior distribution is always non-existent. In this situation, we have to resort to Monte Carlo simulation to sample from the posterior distribution and obtain a numerical approximation accordingly. One popular method to sample from the posterior distribution is Markov chain Monte Carlo (MCMC), which was first introduced by Metropolis et al. [4] and then extended to more general situations by Hastings [5]. In the past decade, many efforts have been devoted to developing more efficient MCMC algorithms, including single-chain and multi-chain methods. One of the most popular single-chain MCMC is delayed rejection adaptive metropolis (DRAM) algorithm developed by Haario et al. [6], which continuously updates the covariance matrix of a Gaussian proposal distribution using the sample path of the chain. However,

when the posterior distribution is multimodal, the performance of single-chain MCMC would always deteriorate [7]. Through running multiple chains in parallel, MCMC can better explore complex posterior distributions with multiple modes. One famous example of multi-chain MCMC is differential evolution adaptive metropolis (DREAM) algorithm developed by Vrugt et al. [8, 9], which has found widespread applications in many different fields since its first introduction [7]. Although MCMC can fully characterize the inherent uncertainties of model parameters, the computational cost needed by MCMC is usually high, especially when the number of unknown parameters is large.

For parameter estimation in high-dimensional problems, a computationally appealing alternative is ensemble Kalman filter (EnKF), which is a Monte Carlo variant of classical Kalman filter [10]. Since its introduction by Evensen [11], EnKF has been widely used in uncertainty quantification of high-dimensional nonlinear problems in oceanic [12, 13], atmospheric [14-16], geophysical [17, 18] and hydrological [19-21] modeling, etc. As a sequential data assimilation method, EnKF needs to modify restart files and update model parameters and states at each assimilation step, which makes its application inconvenient when the model integrates multiple processes [22]. In this situation, computing a global update with all available data is preferred, as in the scheme of ensemble smoother (ES) [23, 24]. Through only updating model parameters, ES can also avoid the inconsistency between updated parameters and states encountered in EnKF. It has been shown that, with much lower computational cost, ES can obtain comparable results as EnKF in some reservoir history matching problems [25]. However, for strongly nonlinear problems, both EnKF [18, 26, 27] and ES [22, 28] need some form of iteration to achieve satisfactory data matches.

As both EnKF and ES rely on the first two statistical moments, they are most suitable for problems with Gaussian distributions. If the distribution of model parameters has multiple modes, using EnKF/ES directly would be problematic. In the last decade, there have been several works trying to solve this problem and extend EnKF/ES to multimodal distributions, most of which are based on clustering analysis. For example, Elsheikh [29] used K-means algorithm, Bengtsson et al. [30] and some

later researchers [31-34] used Gaussian mixture models (GMM) to cluster the samples and update each of the clusters with EnKF/ES. Generally, in these approaches, one has to set the number of clusters in advance, which is rather subtle as the actual number of modes is usually unknown. If the number of modes is large, or there are infinite modes (e.g., using a scalar measurement to estimate a two-dimensional parameter, as shown in the first example of this paper), the performance of clustering analysis may deteriorate. According to Elsheikh [29], another problem is the stochastic nature of clustering analysis, i.e., different runs of the same multimodal inverse algorithm may identify different numbers of modes. Moreover, implementing clustering analysis in high-dimensional problems is challenging. Except for clustering analysis, other ways of dealing with multimodal distributions include integrating EnKF with particle filter (PF) [35] or transforming non-Gaussian variables to Gaussian [36, 37], etc.

In this paper, without resorting to clustering analysis, transformation techniques or another inverse algorithm (e.g., PF), we propose a very simple while efficient algorithm, i.e., the iterative local-updating ensemble smoother (ILUES), to extend ES to multimodal distributions. For each sample in ES, we define a local ensemble based on an integrated measure of distance to this sample and the measurements. Then we use the scheme of ES to update each local ensemble. In this way, the multimodal distributions can be well explored. To achieve satisfactory data matches for strongly nonlinear problems, we adopt an iterative form of ES to assimilate the measurements multiple times. The detailed formulation of the ILUES algorithm is given in section 2. To illustrate its performance, four numerical case studies are tested in section 3. Finally, some conclusions are provided in section 4.

2. Iterative local-updating ensemble smoother

For simplicity, here we represent the system model in the following way:

$$\mathbf{d} = f(\mathbf{m}) + \boldsymbol{\varepsilon}, \quad (1)$$

where \mathbf{d} is a $N_{\mathbf{d}} \times 1$ vector for the measurements, $f(\cdot)$ is the system model, \mathbf{m} is a $N_{\mathbf{m}} \times 1$ vector for the unknown parameters, $\boldsymbol{\varepsilon}$ is a $N_{\mathbf{d}} \times 1$ vector for the measurement

errors. With the noisy measurements \mathbf{d} , we can use ES to update the unknown parameters \mathbf{m} :

$$\mathbf{m}_j^a = \mathbf{m}_j^f + \mathbf{C}_{\text{MD}}^f (\mathbf{C}_{\text{DD}}^f + \mathbf{C}_{\text{D}})^{-1} (\mathbf{d}_j - f(\mathbf{m}_j^f)), \quad (2)$$

for $j = 1, \dots, N_e$.

In the above equation, $\mathbf{M}^f = [\mathbf{m}_1^f, \dots, \mathbf{m}_{N_e}^f]$ is an ensemble of N_e samples that represents our knowledge about the model parameters before assimilating the measurements \mathbf{d} , $\mathbf{M}^a = [\mathbf{m}_1^a, \dots, \mathbf{m}_{N_e}^a]$ is the updated ensemble, \mathbf{C}_{MD}^f is the $N_{\mathbf{m}} \times N_{\mathbf{d}}$ cross-covariance matrix between \mathbf{M}^f and $\mathbf{D}^f = [f(\mathbf{m}_1^f), \dots, f(\mathbf{m}_{N_e}^f)]$, \mathbf{C}_{DD}^f is the $N_{\mathbf{d}} \times N_{\mathbf{d}}$ auto-covariance matrix of \mathbf{D}^f , \mathbf{C}_{D} is the $N_{\mathbf{d}} \times N_{\mathbf{d}}$ covariance matrix for the measurement errors, \mathbf{d}_j is the j th realization of the measurements, $\mathbf{d}_j = \mathbf{d} + \boldsymbol{\varepsilon}_j$.

If the prior or posterior distribution of \mathbf{m} is multimodal, the direct implementation of ES is problematic. Instead of updating \mathbf{M}^f directly according to equation (2), here we propose to update N_e local ensembles of \mathbf{M}^f to extend ES to multimodal distributions. The local ensemble of \mathbf{m}_j^f ($j = 1, \dots, N_e$) is found according to an integrated measure of distance to \mathbf{m}_j^f and the measurements \mathbf{d} :

$$J = J_1 / J_1^{\max} + J_2 / J_2^{\max}, \quad (3)$$

where $J_1 = (f(\mathbf{m}^f) - \mathbf{d})^T \mathbf{C}_{\text{D}}^{-1} (f(\mathbf{m}^f) - \mathbf{d})$, $J_2 = (\mathbf{m}^f - \mathbf{m}_j^f)^T \mathbf{C}_{\text{MM}}^{-1} (\mathbf{m}^f - \mathbf{m}_j^f)$, \mathbf{C}_{MM} is the $N_{\mathbf{m}} \times N_{\mathbf{m}}$ auto-covariance matrix of the model parameters, J_1^{\max} and J_2^{\max} are the maximum values of J_1 and J_2 , respectively. The local ensemble of \mathbf{m}_j^f is the $N_l = \alpha N_e$ ($\alpha \in (0, 1]$) samples with the smallest J values, i.e., $\mathbf{M}_j^{l,f} = [\mathbf{m}_{j,1}^f, \dots, \mathbf{m}_{j,N_l}^f]$. Then according to equation (2), we can update the local ensemble and therefrom select a random sample $\mathbf{m}_j^{l,a}$ as the updated sample corresponding to \mathbf{m}_j^f ($j = 1, \dots, N_e$). In this way, we can better explore the multimodal distribution with the updated global ensemble, $\mathbf{M}^a = [\mathbf{m}_1^{l,a}, \dots, \mathbf{m}_{N_e}^{l,a}]$.

For strongly nonlinear problems, an iterative form of ES is usually needed. In this paper, we adopt the simplest one that assimilates the measurements \mathbf{d} multiple times, which has been integrated into both EnKF [26] and ES [22] for data assimilation in nonlinear problems. In each iteration, we again implement the local updating scheme on the updated ensemble \mathbf{M}^a obtained from the last iteration. After a few iterations, we can obtain good data matches and a converged estimation of the model parameters.

3. Illustrative examples

In this section, we evaluate the ILUES algorithm on four numerical examples with increasing complexity. The first example is quite simple and low-dimensional, which has infinite modes in the posterior distribution and is used to illustrate the basic ideas of the proposed method. To show its applicability in practical problems, we further test the ILUES algorithm with three hydrological examples that have multimodal prior distribution, multimodal posterior distribution and a large number of parameters, respectively.

3.1. Example 1: a simple case with infinite modes in the posterior

The first example tests the ability of the ILUES to identify the posterior distribution with infinite modes, which has the following form:

$$f(x_1, x_2) = x_1^2 + x_2^2. \quad (4)$$

In this case, the prior distributions for x_1 and x_2 are both uniform distributions, $U(-2, 2)$, the scalar measurement is $d = 1$ with measurement error $\varepsilon \sim N(0, 0.01^2)$. It is clear that the posterior distribution for the parameters is close to a round circle with radius equal to \sqrt{d} , which actually means that there are infinite modes. Although this example is rather simple, it is very difficult for the standard ES or the clustering analysis-based ES to solve.

With the ensemble size as $N_e = 400$ and the factor as $\alpha = 0.1$ for the ILUES, the posterior distribution can be well identified within three iterations. The blue dots as shown in Figure 1(a-d) are random samples drawn from the prior distribution and

updated samples obtained from the three iterations, respectively. It is clear that the ILUES algorithm is capable of solving inverse problems with infinite modes in the posterior distributions. Meanwhile, it shows the necessity of assimilating the measurements multiple times to obtain converged results for nonlinear problems.

[Figure 1]

To illustrate the concept of local ensemble, we randomly draw a sample (red diamond) from the prior distribution and plot its local ensemble (black dots) in Figure 1(a). It is shown that the local ensemble actually locates between the original sample and the posterior region, as it is based on an integrated measure of distance to the original sample and the measurement. Applying the updating scheme of ES to this local ensemble, we can obtain an updated sample represented by the red diamond in Figure 1(b), which is much closer to the posterior region. The local ensemble of this updated sample is also plotted with black dots in Figure 1(b). Similar plots are also shown in Figure 1(c-d).

In the above simulation, the factor α is chosen as 0.1. This factor decides the size of the local ensemble. It is understandable that a smaller α would be more suitable for problems with a large number of modes. As we have to make sure that there are enough samples in the local ensemble, given an allowed ensemble size N_e , α cannot be too small. To illustrate the effect of this factor on the performance of the ILUES algorithm, we test nine different values of α and show the corresponding results in Figure 2 (here $N_e = 400$ with three iterations). In this example, as there are infinite modes in the posterior distribution, choosing a large α (e.g., $\alpha > 0.4$) would significantly deteriorate the inversion results. According to our own experience, $\alpha = 0.1$ works well for most of our tested examples and thus it is given as the recommended value.

[Figure 2]

Another setting that affects the performance of the ILUES is the ensemble size N_e . As shown in Figure 3 (here $\alpha = 0.1$ with three iterations), when N_e is small (e.g., $N_e = 50$), we will miss a large portion of the posterior region, which greatly underestimates the uncertainties of the model parameters. When N_e is large (e.g., $N_e = 2000$), we can obtain a pretty good result, but it comes with an increased

computational cost. Generally speaking, a large N_e is needed for a high-dimensional problem or a problem that has a large number of modes, but there is a trade-off between the performance and the computational cost.

[Figure 3]

3.2. Example 2: a rainfall-runoff model with multimodal prior

The second example tests the ability of the ILUES to deal with problems whose prior distributions have multiple modes. Here we consider a more practical case, which is based on a widely used rainfall-runoff model, HYMOD, developed by Boyle [38]. This model connects a simple rainfall-excess model [39] to a series of linear slow and quick reservoirs within a watershed. There are five parameters for HYMOD, i.e., the maximum water storage capacity in the watershed, $C_{max}[L]$, the degree of spatial variability of the soil moisture capacity, $b_{exp}[-]$, the distribution factor for the flow between the slow and the quick reservoirs, $\beta[-]$, the residence time of the slow reservoirs, $R_s[T]$ and the residence time of the quick reservoirs, $R_q[T]$, respectively. In this case, the prior distributions for C_{max} and b_{exp} are $p(C_{max}) = 1/3N(100, 20^2) + 1/3N(250, 20^2) + 1/3N(400, 20^2)$ and $p(b_{exp}) = 1/3N(0.5, 0.1^2) + 1/3N(1, 0.1^2) + 1/3N(1.5, 0.1^2)$, respectively. While the prior distributions for β , R_s and R_q are uniform distributions, whose ranges are listed in Table 1. The stream flow measurements are generated from the true parameters \mathbf{m}^* as listed in Table 1 with additive measurement errors $\boldsymbol{\varepsilon} \sim N(\mathbf{0}, \boldsymbol{\sigma}^2)$, where $\boldsymbol{\sigma} = 0.1f(\mathbf{m}^*)$.

[Table 1]

Choosing the ensemble size as $N_e = 200$ and the factor as $\alpha = 0.1$, the ILUES algorithm can accurately estimate the model parameters within five iterations, as shown in Figure 4. Compared with example 1, although there are more parameters in this example, a smaller N_e is usually capable of quantifying the parametric uncertainties, as the number of modes is not large. However, there is still a trade-off between the performance and the computational cost. If a very small N_e is chosen, there is a risk of obtaining biased inversion results.

[Figure 4]

3.3. Example 3: contaminant source identification with multimodal posterior

In this example, we consider a contaminant source identification problem in steady-state saturated groundwater flow. As shown in Figure 5, the $20[L] \times 10[L]$ domain has constant-head conditions at the left ($12[L]$) and right ($11[L]$) boundaries, no-flow conditions at the lower and upper boundaries, respectively. The conductivity and porosity of the aquifer are homogeneous, whose values are known as $K = 8[LT^{-1}]$ and $\theta = 0.25[-]$, respectively. Then we can obtain a uniform background flow from left to right. In this flow field, some amount of contaminant is released from a point source. The contaminant source is characterized by 5 parameters, $\mathbf{m} = [x_s, y_s, S_s, t_{on}, t_{off}]$, which means that the contaminant is released at $(x_s, y_s)[L]$ from time $t_{on}[T]$ to $t_{off}[T]$ with a constant mass-loading rate $S_s[MT^{-1}]$. The prior distributions for the 5 parameters are uniform, whose ranges are listed in Table 2. To infer these parameters, concentration measurements are collected from a single well denoted by the blue circle in Figure 5 at $t = [6\ 8\ 10\ 12\ 14][T]$ with measurement errors $\varepsilon \sim N(0, 0.01^2)$. The true values of the five parameters that generate the measurements are also listed in Table 2.

[Figure 5]

[Table 2]

The governing equations for the steady-state saturated groundwater flow are:

$$\frac{\partial}{\partial x_i} \left(K_i \frac{\partial h}{\partial x_i} \right) = 0, \quad (5)$$

and

$$v_i = -\frac{K_i}{\theta} \frac{\partial h}{\partial x_i}, \quad (6)$$

where $h[L]$ represents hydraulic head, $K_i[LT^{-1}]$ and $v_i[LT^{-1}]$ represent hydraulic conductivity and pore water velocity along the respective coordinate axis $x_i[L]$ ($i = 1, 2$), respectively.

The advection dispersion equation for the contaminant transport is:

$$\frac{\partial(\theta C)}{\partial t} = \frac{\partial}{\partial x_i} \left(\theta D_{ij} \frac{\partial C}{\partial x_j} \right) - \frac{\partial}{\partial x_i} (\theta v_i C) + q_s C_s, \quad (7)$$

where $C[ML^{-3}]$ represents molar concentration of the dissolved contaminant, $t[T]$ is time, $q_s[T^{-1}]$ and $C_s[ML^{-3}]$ represent flow rate per unit volume of aquifer and concentration of the contaminant source, $D_{ij}[L^2T^{-1}]$ represents hydrodynamic dispersion tensor, whose principal components (D_{xx} and D_{yy}) and cross terms (D_{xy} and D_{yx}) are defined as:

$$\begin{cases} D_{xx} = (\alpha_L v_x^2 + \alpha_T v_y^2) / |v|, \\ D_{yy} = (\alpha_L v_y^2 + \alpha_T v_x^2) / |v|, \\ D_{xy} = D_{yx} = (\alpha_L - \alpha_T) v_x v_y / |v|, \end{cases} \quad (8)$$

where α_L and α_T represent longitudinal and transverse dispersivities, v_x and v_y represent components of the pore water velocity \mathbf{v} along x and y directions, $|v|$ is the magnitude of \mathbf{v} , respectively. Here the longitudinal and transverse dispersivities are known as $\alpha_L = 0.3[L^2T^{-1}]$ and $\alpha_T = 0.03[L^2T^{-1}]$, respectively. The governing equations for the groundwater flow and solute transport are numerically solved with MODFLOW [40] and MT3DMS [41], respectively.

[Figure 6]

To estimate the model parameters, we implement the ILUES algorithm with $N_e = 300$ and $\alpha = 0.1$. As shown in Figure 6, the posterior distribution of y_s is bimodal. To verify that the inversion result obtained by the ILUES algorithm is reasonable, we then run MCMC with the same measurements to obtain a benchmark result. In this case, DREAM algorithm developed by Vrugt is adopted, which has been shown efficient for inverse problems with multimodal distributions [7]. Here we use 8 parallel chains in DREAM algorithm, each of which has a length of 2,000. The Gaussian likelihood function is used to evaluate the goodness-of-fit between model outputs and the measurements. As shown in Figure 7, the trace plots of the model parameters obtained by MCMC are very similar to those obtained by the ILUES algorithm.

[Figure 7]

3.4. Example 4: high-dimensional contaminant source identification

To demonstrate the performance of the ILUES algorithm in high-dimensional inverse problems, we further test a more complex scenario of contaminant source identification. In this example, instead of considering a source with a constant strength, we consider a time-varying source strength, which is characterized by 6 parameters in 6 time segments, i.e., $S_{si}[MT^{-1}]$, $t_i = i:i + 1[T]$, for $i = 1, \dots, 6$. Therefore, along with the source location (x_s, y_s) , there are 8 parameters that characterize the contaminant source. Again, these parameters are assumed to follow uniform distributions, whose ranges are listed in Table 3.

[Table 3]

In this example, we consider the heterogeneity of the conductivity field whose log-transformed values at two arbitrary locations (x_1, y_1) and (x_2, y_2) are assumed to have a separable exponential correlation:

$$C_Y(x_1, y_1; x_2, y_2) = \sigma_Y^2 \exp\left(-\frac{|x_1 - x_2|}{\lambda_x} - \frac{|y_1 - y_2|}{\lambda_y}\right), \quad (9)$$

where $\sigma_Y^2 = 1$ is the variance, $\lambda_x = 10[L]$ and $\lambda_y = 5[L]$ are the correlation lengths along x and y directions, respectively. The Karhunen-Loève (KL) expansion [42] is then used to parameterize the log conductivity field:

$$Y(\mathbf{x}) \approx \bar{Y}(\mathbf{x}) + \sum_{i=1}^{N_{KL}} \sqrt{\tau_i} s_i(\mathbf{x}) \xi_i, \quad (10)$$

where $\bar{Y}(\mathbf{x}) = 2$ is the mean component, τ_i and $s_i(\mathbf{x})$ are eigenvalues and eigenfunctions of the correlation function described in equation (9), $\xi_i (i = 1, \dots, N_{KL})$ are independent standard Gaussian random variables. In this case, 100 KL terms are kept, i.e., $N_{KL} = 100$, which can preserve about 94.7% of the field variance, i.e., $\sum_{i=1}^{100} \tau_i / \sum_{i=1}^{\infty} \tau_i \approx 94.7\%$.

Thus, there are 108 unknown parameters in this case, i.e., the 8 parameters for the contaminant source and the 100 KL terms for the log conductivity field. To infer these parameters, we collect concentration measurements at $t = [4 \ 5 \ 6 \ 7 \ 8 \ 9 \ 10 \ 11 \ 12][T]$ and hydraulic head measurements at the 14 wells denoted by blue squares in Figure 5. The measurement errors for the concentration and hydraulic head are all assumed to

follow $\varepsilon \sim N(0, 0.005^2)$. The reference log conductivity field and true values of source parameters are shown in Figure 9(a) and Table 3, respectively.

[Figure 8]

As this case is high-dimensional, a much larger ensemble size $N_e = 3,000$ is chosen for the ILUES algorithm with $\alpha = 0.1$. As shown in Figure 8, the contaminant source parameters can be accurately identified within 5 iterations. Meanwhile, three realizations, the mean and variance of the posterior log conductivity field are presented in Figure 9(b-f), which clearly demonstrate the estimation accuracy of the log conductivity field.

[Figure 9]

4. Conclusion

In this paper, to extend ensemble smoother to multimodal distributions, we propose a simple while efficient algorithm entitled the iterative local-updating ensemble smoother (ILUES), which is free from clustering analysis. For each sample in ES, we define a local ensemble based on an integrated measure of distance to this sample and the measurements. Then we use the scheme of ES to update each local ensemble. In this way, the multimodal distributions can be well explored. To guarantee the performance of ES in nonlinear problems, a simple iterative form that assimilates the measurements multiple times is adopted. Four numerical case studies are tested to show the performance of the proposed method. The first one verifies the ability of the ILUES algorithm to explore posterior distributions with infinite modes. In this case, we systematically study the effects of original ensemble size and local ensemble size on the performance of the proposed method. The other three case studies are inverse problems in hydrological modeling, which respectively have multiple modes in the prior distribution, multiple modes in the posterior distribution and a large number of unknown parameters. All these four case studies successfully show the performance of the proposed method in adequately quantifying parametric uncertainties of complex systems.

Acknowledgments

Computer codes and data used are available upon request to the first author (zhangjiangjiang.dz@163.com).

This work is supported by the National Natural Science Foundation of China (Grants 41371237 and 41271470).

Jiangjiang Zhang and Weixuan Li would like to acknowledge the support by the Laboratory Directed Research and Development program at Pacific Northwest National Laboratory through the Control of Complex Systems Initiative. Guang Lin would like to acknowledge the support of NSF Grant DMS-1555072 and the U.S. Department of Energy, Office of Science, Office of Advanced Scientific Computing Research, Applied Mathematics program as part of the Multifaceted Mathematics for Complex Energy Systems (M²ACS) project and part of the Collaboratory on Mathematics for Mesoscopic Modeling of Materials project.

We would also like to acknowledge Jasper Vrugt from UC Irvine for providing the codes of DREAM, an efficient MCMC algorithm.

Reference

- [1] J.J. Moré, The Levenberg-Marquardt algorithm: implementation and theory, in: G.A. Watson (Ed.), Numerical Analysis, Lect. Notes Math., vol. 630, Springer-Verlag, Berlin 1978, pp. 105-116.
- [2] K. Deb, A. Pratap, S. Agarwal, T. Meyarivan, A fast and elitist multiobjective genetic algorithm: NSGA-II, IEEE T. Evolut. Comput. , 6 (2) (2002), pp. 182-197 <http://dx.doi.org/10.1109/4235.996017>
- [3] A.M. Stuart, Inverse problems: a Bayesian perspective, Acta Numer., 19 (2010), pp. 451-559 <http://dx.doi.org/10.1017/S0962492910000061>
- [4] N. Metropolis, A.W. Rosenbluth, M.N. Rosenbluth, A.H. Teller, E. Teller, Equation of state calculations by fast computing machines, J. Chem. Phys., 21 (6) (1953), pp. 1087-1092 <http://dx.doi.org/10.1063/1.1699114>
- [5] W.K. Hastings, Monte Carlo sampling methods using Markov chains and their applications, Biometrika, 57 (1) (1970), pp. 97-109 <http://dx.doi.org/10.1093/biomet/57.1.97>
- [6] H. Haario, M. Laine, A. Mira, E. Saksman, DRAM: efficient adaptive MCMC, Stat. Comput., 16 (4) (2006), pp. 339-354 <http://dx.doi.org/10.1007/s11222-006-9438-0>
- [7] J.A. Vrugt, Markov chain Monte Carlo simulation using the DREAM software package: Theory, concepts, and MATLAB implementation, Environ. Modell. Softw., 75 (2016), pp. 273-316
- [8] J.A. Vrugt, C.J. Ter Braak, M.P. Clark, J.M. Hyman, B.A. Robinson, Treatment of input uncertainty in hydrologic modeling: Doing hydrology backward with Markov chain Monte Carlo simulation, Water Resour. Res., 44 (12) (2008), pp. W00B09 <http://dx.doi.org/10.1029/2007WR006720>
- [9] J.A. Vrugt, C. Ter Braak, C. Diks, B.A. Robinson, J.M. Hyman, D. Higdon, Accelerating Markov chain Monte Carlo simulation by differential evolution with self-adaptive randomized subspace sampling, Int. J. Nonlin. Sci. Num., 10 (3) (2009), pp. 273-290 <http://dx.doi.org/10.1515/IJNSNS.2009.10.3.273>
- [10] R.E. Kalman, A new approach to linear filtering and prediction problems, J. Basic Eng., 82 (1) (1960), pp. 35-45 <http://dx.doi.org/10.1115/1.3662552>
- [11] G. Evensen, Sequential data assimilation with a nonlinear quasi-geostrophic model using Monte Carlo methods to forecast error statistics, J. Geophys. Res., 99 (C5) (1994), pp. 10143-10162 <http://dx.doi.org/10.1029/94JC00572>
- [12] L. Bertino, G. Evensen, H. Wackernagel, Sequential data assimilation techniques in oceanography, Int. Stat. Rev., 71 (2) (2003), pp. 223-241 <http://dx.doi.org/10.1111/j.1751-5823.2003.tb00194.x>
- [13] C.L. Keppenne, M.M. Rienecker, Assimilation of temperature into an isopycnal ocean general circulation model using a parallel ensemble Kalman filter, J. Mar. Syst., 40 (2003), pp. 363-380 [http://dx.doi.org/10.1016/S0924-7963\(03\)00025-3](http://dx.doi.org/10.1016/S0924-7963(03)00025-3)
- [14] P.L. Houtekamer, H.L. Mitchell, A sequential ensemble Kalman filter for atmospheric data assimilation, Mon. Weather Rev., 129 (1) (2001), pp. 123-137 [http://dx.doi.org/10.1175/1520-0493\(2001\)129<0123:ASEKFF>2.0.CO;2](http://dx.doi.org/10.1175/1520-0493(2001)129<0123:ASEKFF>2.0.CO;2)
- [15] E. Ott, B.R. Hunt, I. Szunyogh, A.V. Zimin, E.J. Kostelich, M. Corazza, E. Kalnay, D. Patil, J.A. Yorke, A local ensemble Kalman filter for atmospheric data assimilation, Tellus A, 56 (5) (2004), pp. 415-428 <http://dx.doi.org/10.1111/j.1600-0870.2004.00076.x>
- [16] P. Houtekamer, F. Zhang, Review of the ensemble Kalman filter for atmospheric data assimilation, Mon. Weather Rev., (2016) (2016), <http://dx.doi.org/10.1175/MWR-D-15-0440.1>
- [17] S.I. Aanonsen, G. Nævdal, D.S. Oliver, A.C. Reynolds, B. Vallès, The ensemble Kalman filter in reservoir engineering-a review, SPE J., 14 (03) (2009), pp. 393-412 <http://dx.doi.org/10.2118/117274-PA>

- [18] Y. Gu, D.S. Oliver, An iterative ensemble Kalman filter for multiphase fluid flow data assimilation, SPE J., 12 (04) (2007), pp. 438-446 <http://dx.doi.org/10.2118/108438-PA>
- [19] H. Moradkhani, S. Sorooshian, H.V. Gupta, P.R. Houser, Dual state-parameter estimation of hydrological models using ensemble Kalman filter, Adv. Water Res., 28 (2) (2005), pp. 135-147 <http://dx.doi.org/10.1016/j.advwatres.2004.09.002>
- [20] R.H. Reichle, D.B. McLaughlin, D. Entekhabi, Hydrologic data assimilation with the ensemble Kalman filter, Mon. Weather Rev., 130 (1) (2002), pp. 103-114 [http://dx.doi.org/10.1175/1520-0493\(2002\)130<0103:HDAWTE>2.0.CO;2](http://dx.doi.org/10.1175/1520-0493(2002)130<0103:HDAWTE>2.0.CO;2)
- [21] Y. Chen, D. Zhang, Data assimilation for transient flow in geologic formations via ensemble Kalman filter, Adv. Water Res., 29 (8) (2006), pp. 1107-1122 <http://dx.doi.org/10.1016/j.advwatres.2005.09.007>
- [22] A.A. Emerick, A.C. Reynolds, Ensemble smoother with multiple data assimilation, Comput. Geosci., 55 (2013), pp. 3-15 <http://dx.doi.org/10.1016/j.cageo.2012.03.011>
- [23] P.J. Van Leeuwen, G. Evensen, Data assimilation and inverse methods in terms of a probabilistic formulation, Mon. Weather Rev., 124 (12) (1996), pp. 2898-2913 [http://dx.doi.org/10.1175/1520-0493\(1996\)124<2898:DAAIMI>2.0.CO;2](http://dx.doi.org/10.1175/1520-0493(1996)124<2898:DAAIMI>2.0.CO;2)
- [24] G. Evensen, Data assimilation: the ensemble Kalman filter, Springer-Verlag, Berlin 2007.
- [25] J.-A. Skjervheim, G. Evensen, An ensemble smoother for assisted history matching, in: SPE Reservoir Simulation Symposium, Society of Petroleum Engineers, The Woodlands, Texas, 2011, <http://dx.doi.org/10.2118/141929-MS>
- [26] R.J. Lorentzen, G. Naevdal, An iterative ensemble Kalman filter, IEEE T. Automat. Contr., 56 (8) (2011), pp. 1990-1995 <http://dx.doi.org/10.1109/TAC.2011.2154430>
- [27] A.A. Emerick, A.C. Reynolds, History matching time-lapse seismic data using the ensemble Kalman filter with multiple data assimilations, Computat. Geosci., 16 (3) (2012), pp. 639-659 <http://dx.doi.org/10.1007/s10596-012-9275-5>
- [28] Y. Chen, D.S. Oliver, Ensemble randomized maximum likelihood method as an iterative ensemble smoother, Math. Geosci., 44 (1) (2012), pp. 1-26 <http://dx.doi.org/10.1007/s11004-011-9376-z>
- [29] A.H. Elsheikh, M.F. Wheeler, I. Hoteit, Clustered iterative stochastic ensemble method for multimodal calibration of subsurface flow models, J. Hydrol., 491 (2013), pp. 40-55 <http://dx.doi.org/10.1016/j.jhydrol.2013.03.037>
- [30] T. Bengtsson, C. Snyder, D. Nychka, Toward a nonlinear ensemble filter for high-dimensional systems, J. Geophys. Res., 108 (D24) (2003), <http://dx.doi.org/10.1029/2002JD002900>
- [31] K.W. Smith, Cluster ensemble Kalman filter, Tellus Ser. A, 59 (5) (2007), pp. 749-757 <http://dx.doi.org/10.1111/j.1600-0870.2007.00246.x>
- [32] L. Dovera, E. Della Rossa, Multimodal ensemble Kalman filtering using Gaussian mixture models, Computat. Geosci., 15 (2) (2011), pp. 307-323 <http://dx.doi.org/10.1007/s10596-010-9205-3>
- [33] R. Li, V. Prasad, B. Huang, Gaussian Mixture Model-Based Ensemble Kalman Filtering for State and Parameter Estimation for a PMMA Process, Processes, 4 (2) (2016), pp. 9 <http://dx.doi.org/10.3390/pr4020009>
- [34] A.Y. Sun, A.P. Morris, S. Mohanty, Sequential updating of multimodal hydrogeologic parameter fields using localization and clustering techniques, Water Resour. Res., 45 (7) (2009), <http://dx.doi.org/10.1029/2008WR007443>
- [35] J. Mandel, J.D. Beezley, An ensemble Kalman-particle predictor-corrector filter for non-Gaussian data assimilation, in: International Conference on Computational Science, Springer-Verlag, Berlin, 2009, pp. 470-478 http://dx.doi.org/10.1007/978-3-642-01973-9_53

- [36] E. Simon, L. Bertino, Application of the Gaussian anamorphosis to assimilation in a 3-D coupled physical-ecosystem model of the North Atlantic with the EnKF: a twin experiment, *Ocean Sci.*, 5 (4) (2009), pp. 495-510 <http://dx.doi.org/10.5194/os-5-495-2009>
- [37] H. Zhou, J.J. Gomez-Hernandez, H.-J.H. Franssen, L. Li, An approach to handling non-Gaussianity of parameters and state variables in ensemble Kalman filtering, *Adv. Water Resour.*, 34 (7) (2011), pp. 844-864 <http://dx.doi.org/10.1016/j.advwatres.2011.04.014>
- [38] D.P. Boyle, Multicriteria calibration of hydrologic models, Ph.D. dissertation, in: Dep. of Hydrol. and Water Resour., Univ. of Ariz., Tucson, 2000, <http://arizona.openrepository.com/arizona/handle/10150/290657>
- [39] R. Moore, The probability-distributed principle and runoff production at point and basin scales, *Hydrol. Sci. J.*, 30 (2) (1985), pp. 273-297 <http://dx.doi.org/10.1080/02626668509490989>
- [40] A.W. Harbaugh, E.R. Banta, M.C. Hill, M.G. McDonald, MODFLOW-2000, The U. S. Geological Survey Modular Ground-Water Model-User Guide to Modularization Concepts and the Ground-Water Flow Process, in: Open-file Report. U.S. Geol. Survey, Reston,VA, 2000, http://wipp.energy.gov/library/cra/2009_cra/references/Others%5CHarbaugh_Banta_Hill_and_McDonald_2000_MODFLOW_2000_Open_File_Report_00_92.pdf
- [41] C. Zheng, P.P. Wang, MT3DMS: a modular three-dimensional multispecies transport model for simulation of advection, dispersion, and chemical reactions of contaminants in groundwater systems; documentation and user's guide, in, DTIC Document, 1999, <http://oai.dtic.mil/oai/oai?verb=getRecord&metadataPrefix=html&identifier=ADA373474>
- [42] D. Zhang, Z. Lu, An efficient, high-order perturbation approach for flow in random porous media via Karhunen–Loeve and polynomial expansions, *J. Comput. Phys.*, 194 (2) (2004), pp. 773-794 <http://dx.doi.org/10.1016/j.jcp.2003.09.015>

Table and Figures

Table 1 Prior ranges and true values of model parameters for the second example

Parameter	$C_{max}[L]$	$b_{exp}[-]$	$\beta[-]$	$R_s[L]$	$R_q[L]$
Range	[1 500]	[0.1 2]	[0.1 0.99]	[0 0.1]	[0.1 0.99]
True value	409.1018	1.5430	0.8998	0.0233	0.7232

Table 2 Prior ranges and true values of model parameters for the third example

Parameter	$x_s[L]$	$y_s[L]$	$S_s[MT^{-1}]$	$t_{on}[T]$	$t_{off}[T]$
Range	[3 5]	[3 7]	[10 13]	[3 5]	[9 11]
True value	3.8537	5.9994	11.0442	4.8966	9.0745

Table 3 Prior ranges and true values of contaminant source parameters for the fourth example

Parameter	Range	True value
$x_s[L]$	[3 5]	3.5196
$y_s[L]$	[4 6]	4.4366
$S_{s1}[MT^{-1}]$	[0 8]	5.6916
$S_{s2}[MT^{-1}]$	[0 8]	7.8833
$S_{s3}[MT^{-1}]$	[0 8]	6.3064
$S_{s4}[MT^{-1}]$	[0 8]	1.4852
$S_{s5}[MT^{-1}]$	[0 8]	6.8717
$S_{s6}[MT^{-1}]$	[0 8]	5.5517

Figure 1. (a) Random samples drawn from the prior distribution and (b-d) updated samples obtained from three iterations. The local ensemble (black dots) of a sample denoted by the red diamond is shown in each subplot.

Figure 2. With different values of the factor α , the obtained results of parameter estimation. Here the ensemble size is $N_e=400$.

Figure 3. With different values of the ensemble size N_e , the obtained results of parameter estimation. Here $\alpha = 0.1$.

Figure 4. Trace plots of model parameters obtained from the ILUES algorithm in the second example. Here $N_e=200$ and $\alpha = 0.1$.

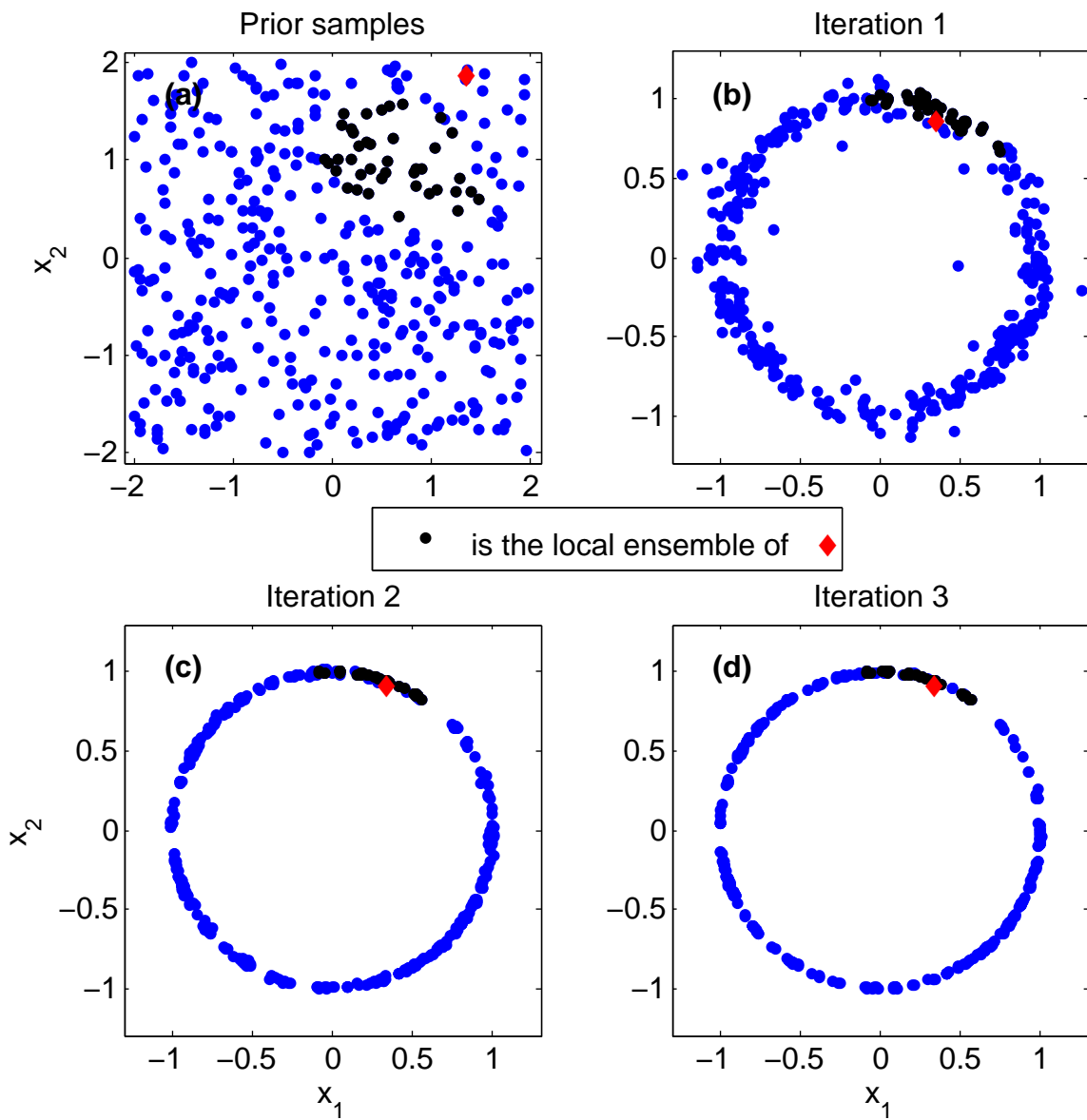
Figure 5. Flow domain for the third and fourth examples. The potential area of the contaminant source is represented with the red dashed rectangle. The measurement locations for the third and fourth examples are demoted by blue circle and blue squares, respectively.

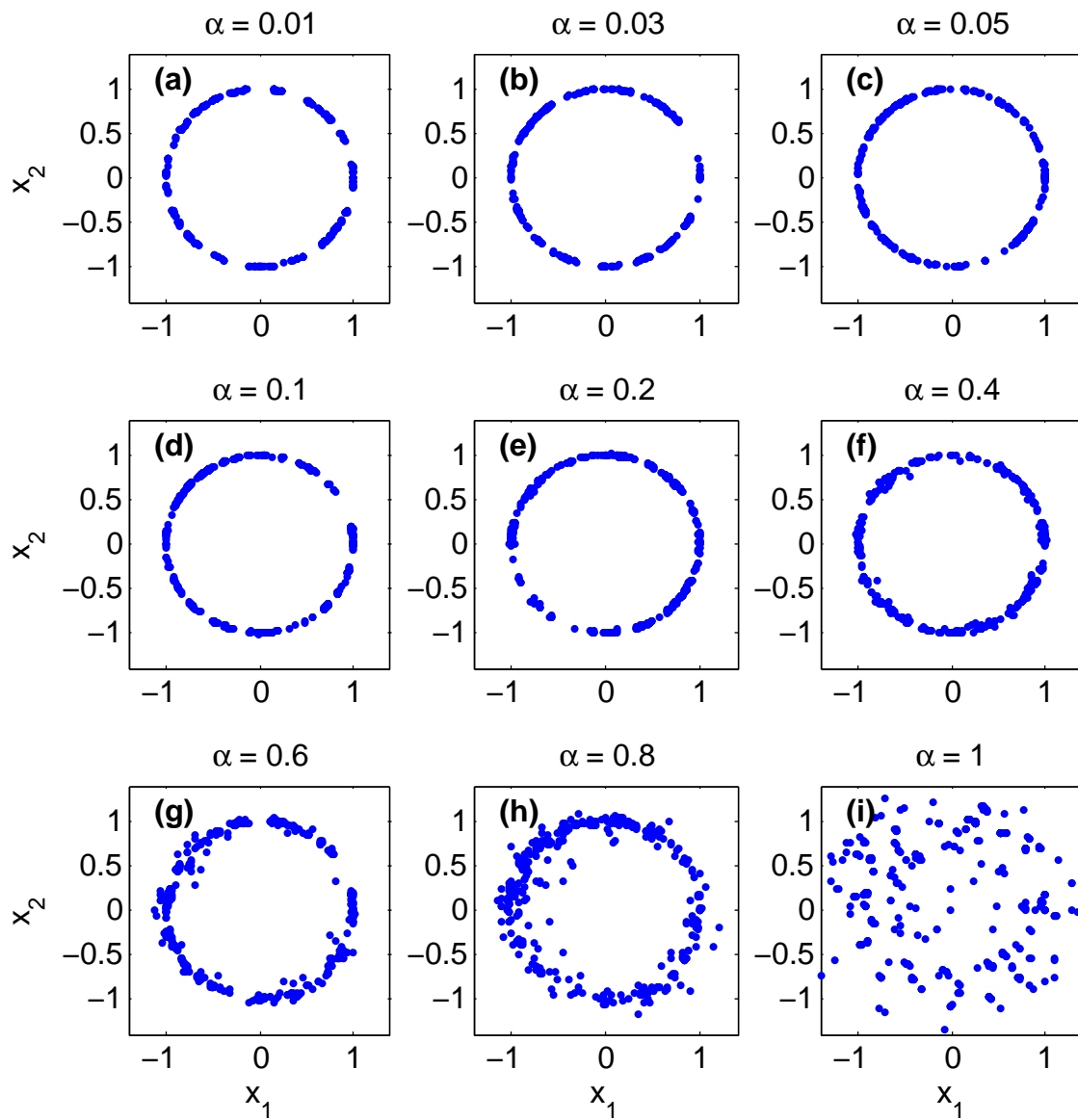
Figure 6. Trace plots of model parameters obtained from the ILUES algorithm in the third example. Here $N_e=300$ and $\alpha = 0.1$.

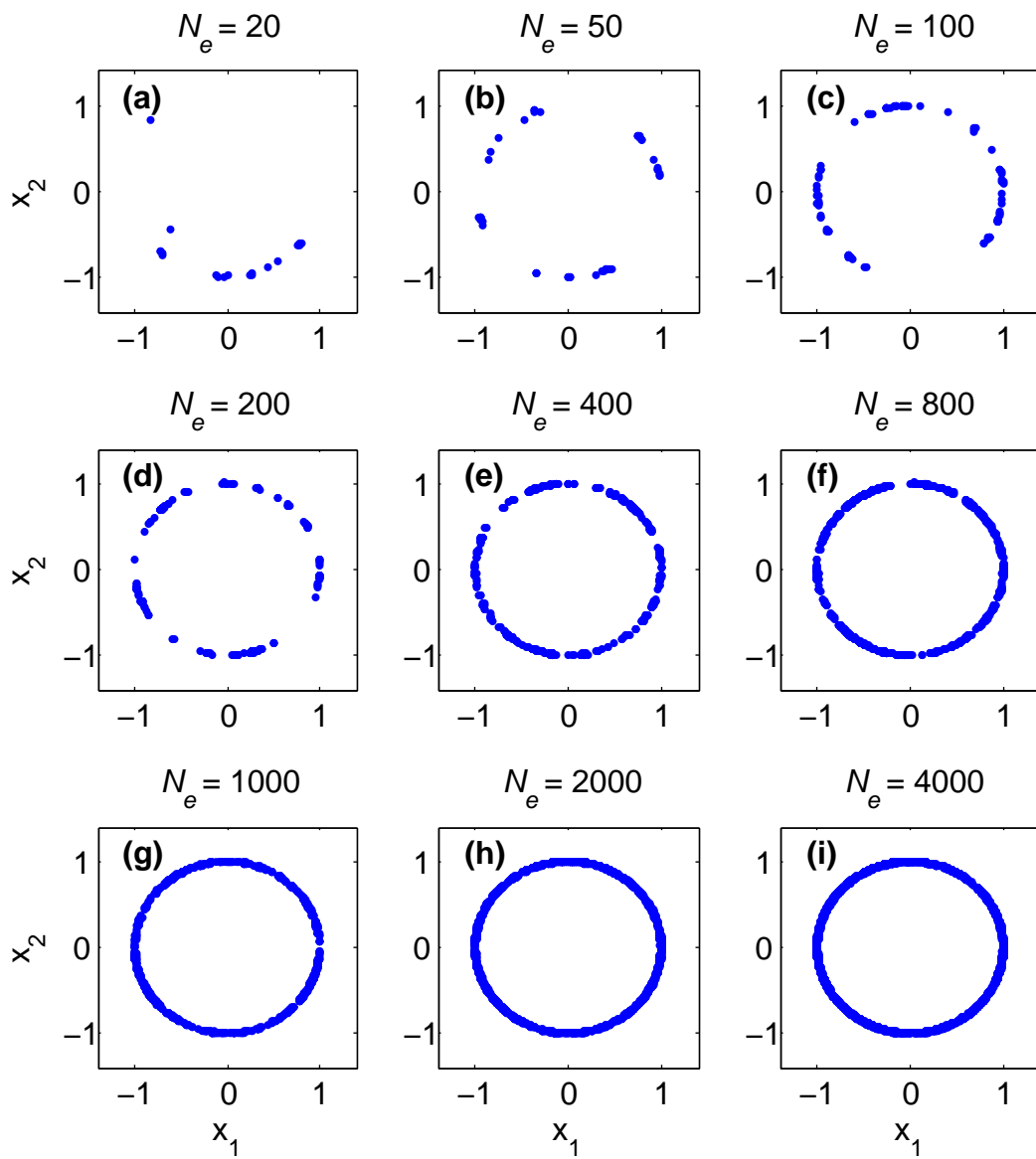
Figure 7. Trace plots of model parameters obtained from DREAM algorithm in the third example.

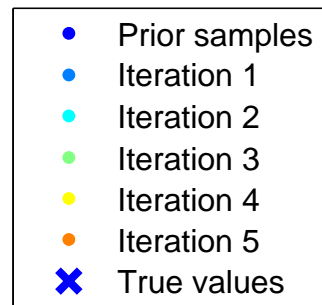
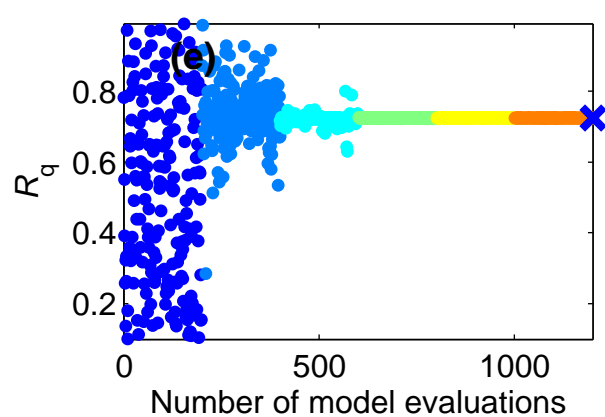
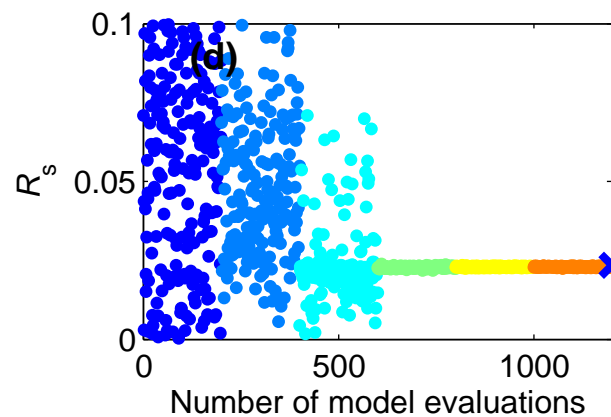
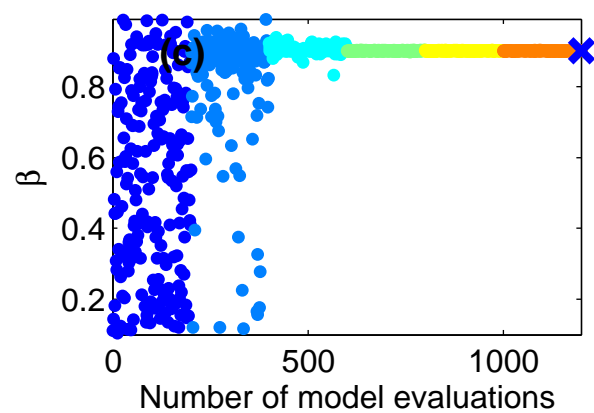
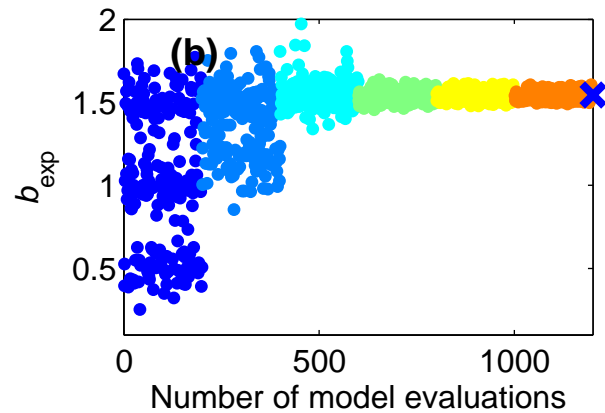
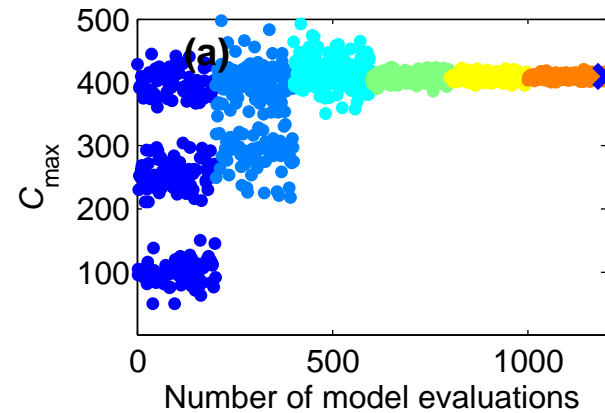
Figure 8. Trace plots of contaminant source parameters obtained from the ILUES algorithm in the fourth example. Here $N_e=3000$ and $\alpha = 0.1$.

Figure 9. (a) Reference log conductivity field, (b-d) three posterior realizations of the log conductivity field, (e) mean estimate of the log conductivity field and (f) estimation variance of the log conductivity field.

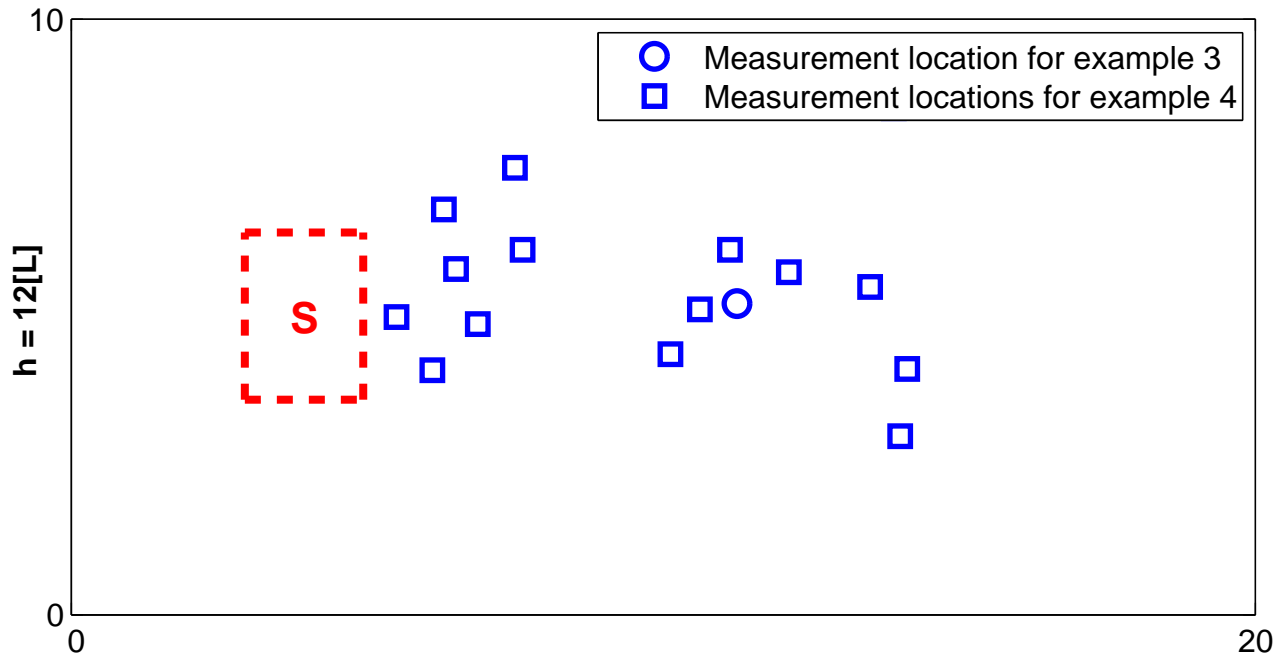








No flow



$h = 12[L]$

$h = 11[L]$

No flow

20

0

